

Section 1

LASER SYSTEM REPORT

1.A GDL Facility Report

GDL has been shut down for the complete replacement of the front end with the actively mode-locked, Q-switched (AMQ) oscillator and predriver. Work has continued throughout this period on activation and alignment of the oscillator, a refurbishment of the active mirror system, and complete system realignment. A portion of the GDL downtime was caused by construction efforts to cut holes for the 25th-beam project and installation of the periscope. (The beam will be used for creating an x-ray backlighting source for OMEGA experiments.) Plans call for activation of the system to support NLUF experiments during July.

ACKNOWLEDGMENT

This work was supported by the U.S. Department of Energy Office of Inertial Fusion under agreement number DE-FC08-85DP40200 and by the Laser Fusion Feasibility Project at the Laboratory for Laser Energetics, which has the following sponsors: Empire State Electric Energy Research Corporation, General Electric Company, New York State Energy Research and Development Authority, Northeast Utilities Service Company, Ontario Hydro, Southern California Edison Company, The Standard Oil Company, and University of Rochester. Such support does not imply endorsement of the content by any of the above parties.

1.B OMEGA Facility Report

The OMEGA laser system has operated this entire quarter as a fully ultraviolet, 24-beam irradiation facility. Initial experiments were performed to examine neutron yield, thermal transport, and uniformity of irradiation. During system checkout, a record neutron yield of 2×10^{11} was obtained. Collaborative experiments with other laboratories (Los Alamos National Laboratory, University of Florida, and University of Maryland), through the National Laser Users Facility, examined different aspects of x-ray physics.

In parallel with the experiments, the newly UV-converted system was adjusted for energy balance between beams, beam alignment, and energy output. Energies on target were typically greater than 2 kJ, with a maximum of 2.42 kJ. Energy variation among the beams was at the 5% level, with the smallest variation 3.4%. At times, a multishift operation was used to attain a shot rate of 30 to 40 per week in support of the thermal transport studies and the x-ray conversion studies.

Many new diagnostic instruments were activated during this period, including four independent x-ray streak cameras. Progress was made toward successfully activating a time fiducial on the elliptical crystal streak spectrograph using a portion of the driver-line output, which was transported to the target chamber ahead of the main beams, converted to the fourth harmonic (175 nm), and directed to the camera via fiber optics. In collaboration with Los Alamos National Laboratory (LANL), progress was also made to activate the miniflex x-ray diode system. An experimental systems operator was added to streamline experimental operation of the system; this led to a substantial increase in the shot rate.

The facility work was completed for the 25th-beam project, and the periscope to elevate the GDL output beam to the OMEGA target bay level was installed. Installation of the 25th beam is planned for July and August. The AMQ oscillator project is on schedule for OMEGA installation in late July.

A summary of OMEGA operations this quarter follows:

| | | |
|-----------------------------|--------------|-------------------|
| Driver Shots | 43 | (11%) |
| Beamline Test Shots | 7 | (2%) |
| Software Tests and Failures | 43 | (11%) |
| Target Shots | 294 | (76%) |
| | TOTAL | 387 (100%) |

ACKNOWLEDGMENT

This work was supported by the U.S. Department of Energy Office of Inertial Fusion under agreement number DE-FC08-85DP40200 and by the Laser Fusion Feasibility Project at the Laboratory for Laser Energetics, which has the following sponsors: Empire State Electric Energy Research Corporation, General Electric Company, New York State Energy Research and Development Authority, Northeast Utilities Service Company, Ontario Hydro, Southern California Edison Company, The Standard Oil Company, and University of Rochester. Such support does not imply endorsement of the content by any of the above parties.

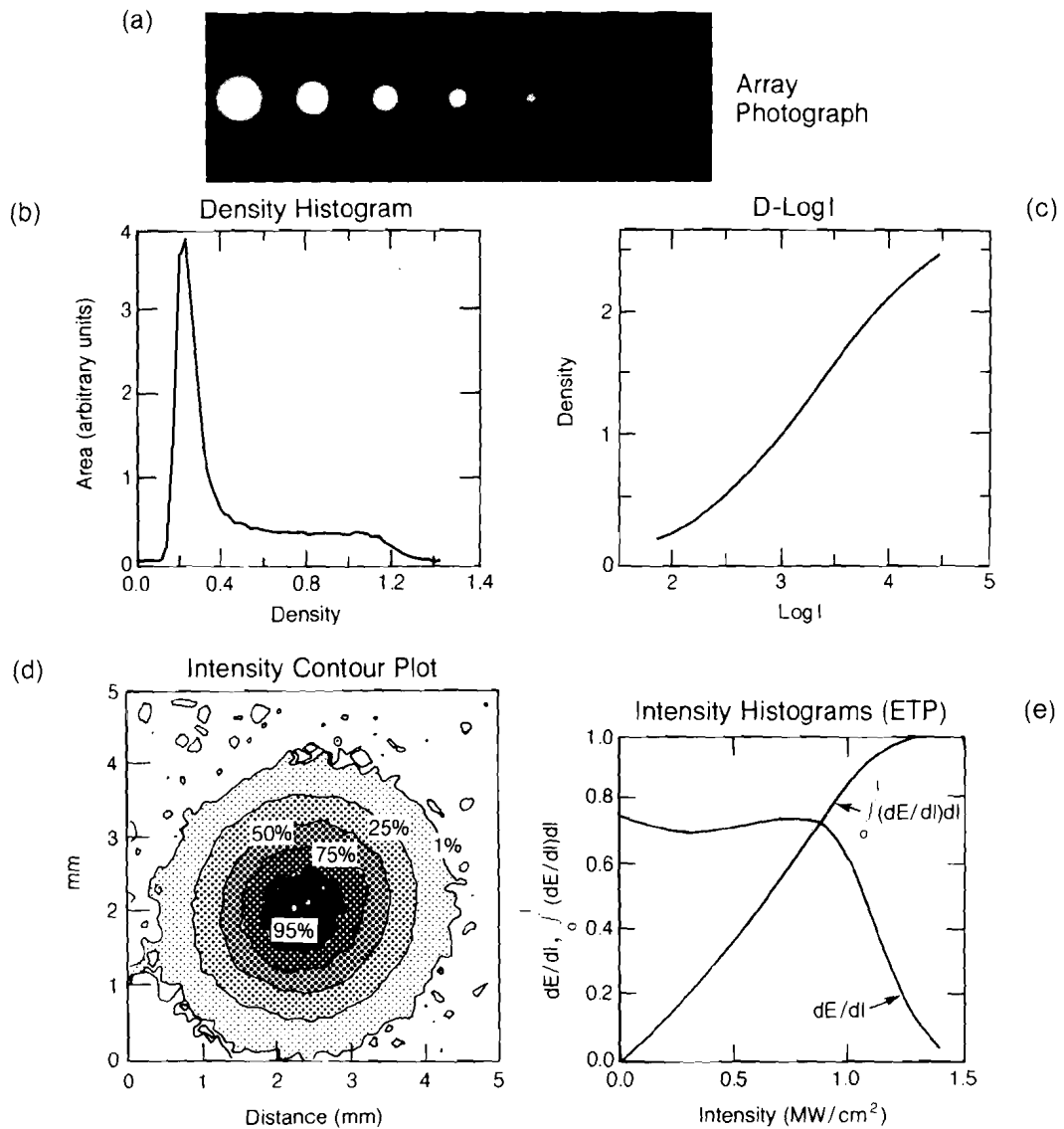
1.C OMEGA Uniformity Program

It is expected that fluctuations in laser intensity over the target surface must be kept below a few percent to drive high-density implosions. Although various theoretical^{1,2} and experimental^{3,4} aspects of irradiation uniformity have been under investigation for several years, the need for high-quality laser-beam profiles has not been a crucial issue, as high-density implosions have not been possible. The 24-beam IR implosion experiments³ were relatively insensitive to illumination nonuniformity due to the smoothing action of the copious amounts of fast electrons from resonance absorption, but these electrons also preheated the target, preventing high compression. The 6-beam UV implosion experiments⁴ were free of fast electrons, but they were dominated by the large nonuniformity inherent in the 6-beam geometry. However, the 24-beam UV irradiation now available on OMEGA removes a great part of this inherent geometrical contribution to nonuniformity, and opens the possibility for high-density ablative implosions if good beam quality can be achieved. Smooth beam profiles are possible and have been obtained on the GDL system.² There is now a strongly increased effort to quantitatively assess and improve the beam quality on OMEGA.

In order to translate the hydrodynamic uniformity requirements into laser beam quality requirements, we have developed a three-dimensional (3-D) beam superposition code. This code permits the input of two-dimensional (2-D), digitized images for each of the 24 beams of OMEGA, or for any arbitrary profile. Studies were performed to assess the sensitivity of target irradiation to particular types of illumination nonuniformity, such as noncircularity, irregularities in beam profiles, target misalignment, beam energy imbalance, and mispointing of beams on target. The output of this code yields overall rms fluctuations as well as the amplitudes of a spherical harmonic decomposition of the nonuniformity. The results can be summarized as follows: beam energy imbalance, mispointing, and noncircular beams all contribute to ℓ -modes below $\ell = 4$. Beam profile fluctuations, on the other hand, predominantly contribute to modes with $\ell \geq 8$. Purely geometrical effects related to beam overlap for the 24-beam OMEGA illumination configuration predominantly produce modes with $\ell = 8-12$, even for perfect beams.

Experimentally, the capability of measuring individual beam energies to an accuracy of 1% has been developed, and beam energy balance in the 2 to 3% range is now achievable. With refinements, a 1% beam energy balance can be envisaged. Similarly, mispointing on target can easily be kept within 10 to 20 μ rad, which is considered adequate for high-density implosions. The remaining laser beam characteristic enhancing low-order ℓ -modes, the beam circularity, relates mostly to laser alignment. As such, appropriate alignment procedures should bring this problem well within tolerable limits.

With a number of uniformity issues removed, the main thrust of the uniformity program at LLE involves assessment and improvement of the individual laser beam profiles with their superposed, more or less random intensity fluctuations. The theoretical requirement for beam quality is to approach a quadratic intensity profile with intensity fluctuations not exceeding 20% peak to valley.²



E3487

Fig. 23.1
 Image processing. (a) Array photograph with successive images attenuated by factors of 2. (b) Density histogram of one of the images. Using two density histograms of the images in (a) we obtain film intensity response curves (D-log I) shown in (c). An intensity contour plot of an expanded oscillator beam is shown in (d). The corresponding intensity histogram (dE/dI vs I) as well as its integrated counterpart are shown in (e). The flat histogram is close to the rectangular histogram expected for a Gaussian beam.

In order to assess the beam quality on target accurately, we have re-examined laser performance by photographing the laser beams in the near field (at the output of the laser system), as well as in the equivalent target plane of an auxiliary focusing lens, with a much longer focal length than the actual OMEGA focusing lenses. This arrangement⁵ leads to satisfactory mapping of the on-target intensity distribution if the actual focusing lenses are close to diffraction limited. The quantitative analysis of these photographs involves a recently acquired Perkin-Elmer 2-D microdensitometer along with computerized image analysis codes. This analysis includes a D-logI intensity response conversion, contour plotting, and intensity histograms. Figure 23.1 illustrates the process, from taking array photographs of an image, to density histograms, intensity response curves (D-logI), contour plots, and intensity histograms. While size and symmetry properties can be obtained conveniently from contour plots, the intensity histogram (dE/dI vs I) shown in Fig. 23.1(e) frequently yields very useful data for the interpretation of laser-fusion experiments (average and peak intensities, etc.) as well as for rapid evaluation of the on-target irradiation nonuniformity. Since Fig. 23.1 is an image of the oscillator output, it approximates very closely a Gaussian profile, for which the intensity histogram (dE/dI vs I) is a rectangle.

The intensity distribution in the target plane (quasi far field) depends on the intensity and phase distribution of the beam incident on the focusing optics. A smooth near-field beam intensity distribution, as shown in Fig. 23.2, is therefore a requirement for a smooth equivalent-target-plane (ETP) intensity distribution. However, the detailed phase

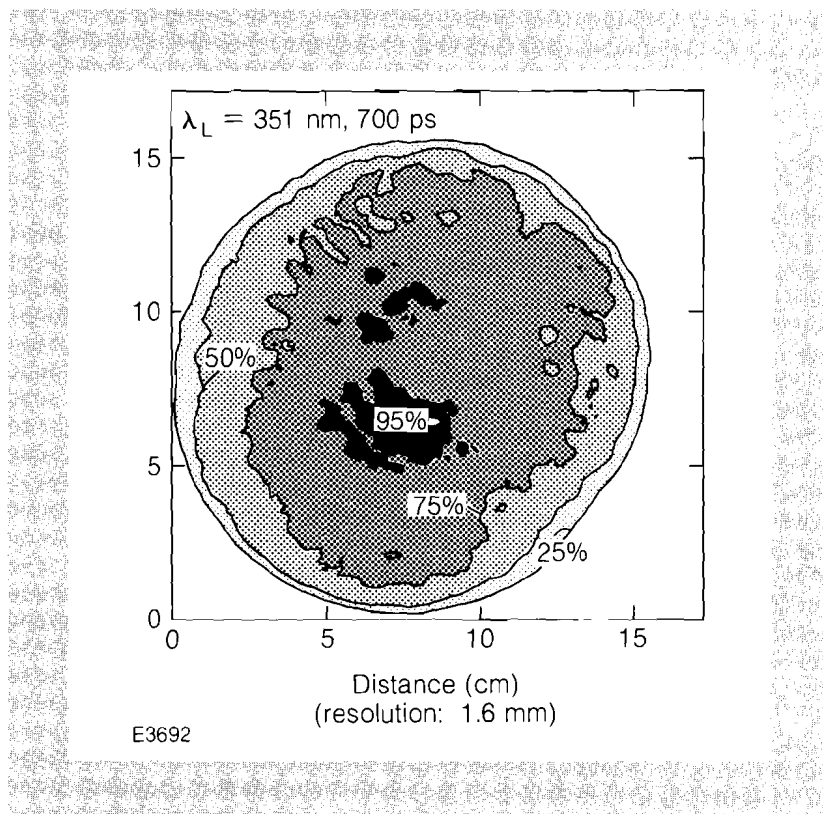
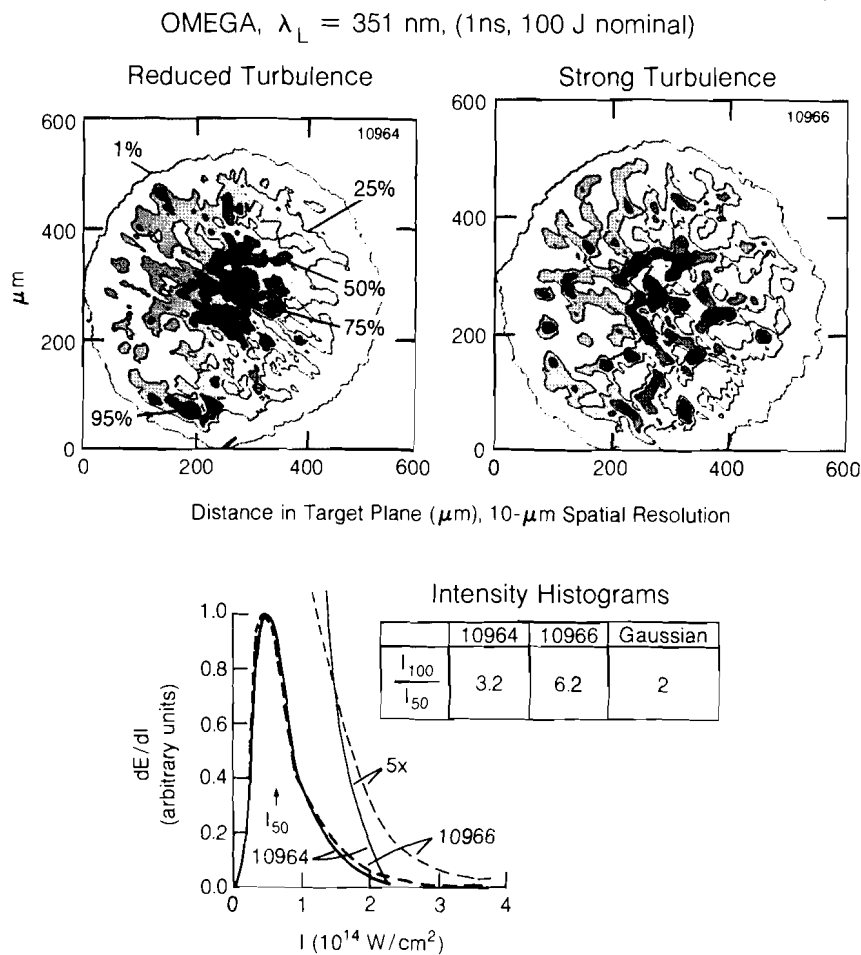


Fig. 23.2
Intensity contour plot of a UV near-field image at the output of the up-conversion crystal in OMEGA.

front distribution of this beam is very difficult to measure, and frequently the ETP distribution is taken instead. Figure 23.3 shows two such ETP contour plots with their corresponding intensity histograms. The effect of air turbulence is shown: one image is under normal operating conditions and the other has reduced turbulence. While the median intensity in the two images is roughly equal, the ratio of maximum to median intensity is approximately two times larger for the beam suffering from strong air turbulence. The 3-D superposition code (using the same beam profiles for all 24 beams of OMEGA) also showed that the rms nonuniformity for the poorer beam profile resulted in an rms nonuniformity over the target surface of roughly twice that for the case with reduced turbulence ($\sigma_{rms} \approx 30\%$ and 15% , respectively).



E3484

Fig. 23.3
Equivalent-target-plane intensity distributions for one of the OMEGA UV beams with strong and reduced air turbulence. The effect of reducing air turbulence is particularly evident in the histograms, where it leads to a peak-to-median intensity ratio that is half as large as the one for strong turbulence. The effect of increased turbulence manifests itself in increased intensity gradients and patchy contour plots.

Analysis of the up-conversion crystals⁶ also showed that many of them contribute significantly to the phase-front distortions on the beams, particularly in the form of small-scale phase gradients. Figure 23.4 is a demonstration of how different crystals affect the ETP intensity distribution of an auxiliary 351-nm alignment beam [Fig. 23.4(a)]. The best up-conversion cell available at LLE hardly changes the ETP contour plot or intensity histogram over that of the undisturbed alignment beam [compare Figs. 23.4(a) and 23.4(b)], while the worst crystal assembly leads to dramatic changes [Figs. 23.4(c) and 23.4(d)]. In particular, the intensity histogram shows a maximum intensity that is twice that of the ETP of the undisturbed alignment beam. Here, too, the 3-D superposition code showed that the rms intensity fluctuations of the 24 beams of OMEGA on the target are approximately two times worse

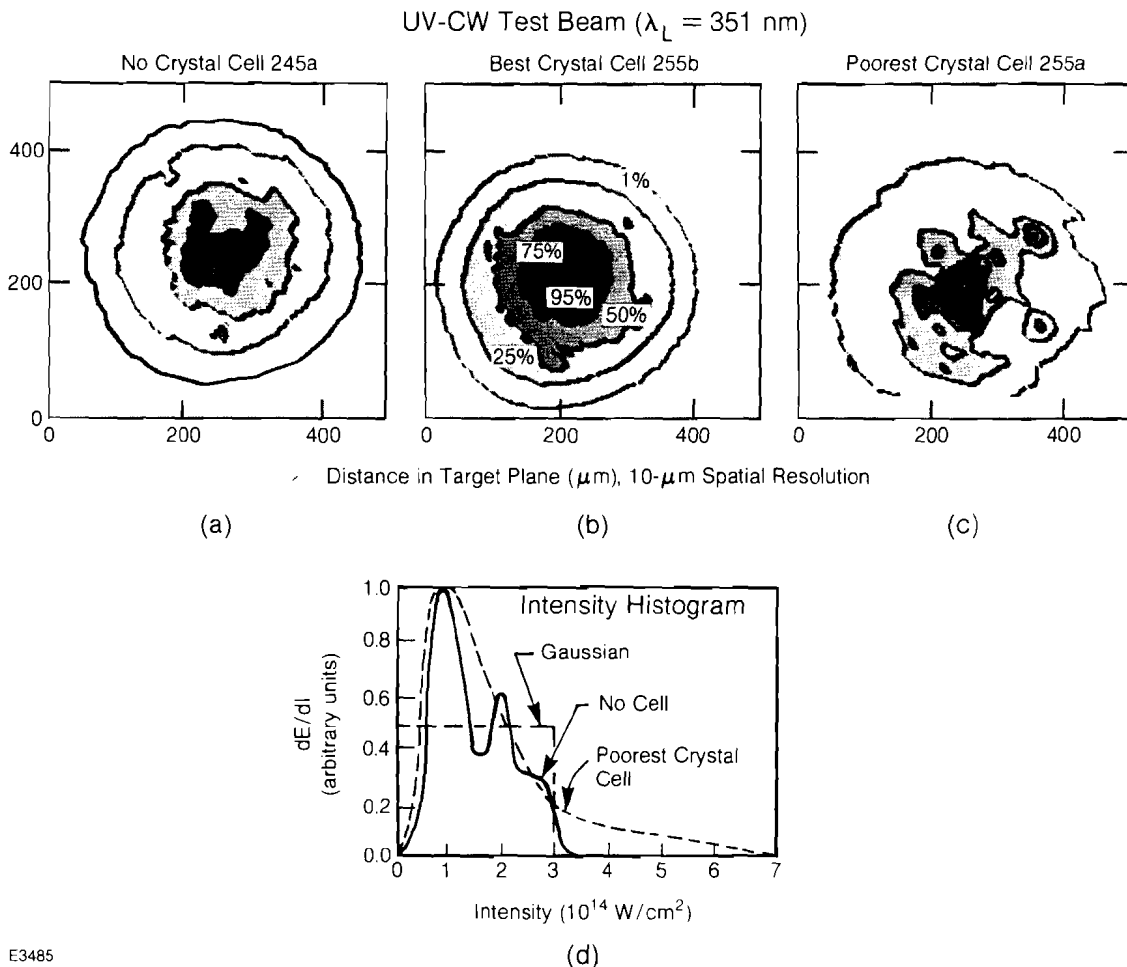


Fig. 23.4

Effect of different up-conversion crystal cells on equivalent-target-plane intensity distributions. The ETP contour plot of an auxiliary cw UV alignment beam is shown in (a). The best LLE up-conversion cell hardly affects this distribution (b), while the worst cell strongly distorts the distribution (c) and increases the peak-to-median intensity ratio (d) by a factor of 2.

when the intensity distribution of Fig. 23.4(c) was used, as compared to Fig. 23.4(a) ($\sigma_{rms} \geq 10\%$ and 5% , respectively).

The results shown above suggest a near-term uniformity program that concentrates on problems related to air turbulence, beam propagation, and crystal quality. The longer-term program focuses on the intrinsic laser performance and its improvements. This includes the implementation on OMEGA of the recently developed holographic method for analyzing the phase distribution in the near field of the laser output.⁷ In addition, a low-level effort is under way to study the feasibility of using random phase plates⁸ or their equivalent to increase the average on-target illumination uniformity.

ACKNOWLEDGMENT

This work was supported by the U.S. Department of Energy Office of Inertial Fusion under agreement number DE-FC08-85DP40200 and by the Laser Fusion Feasibility Project at the Laboratory for Laser Energetics, which has the following sponsors: Empire State Electric Energy Research Corporation, General Electric Company, New York State Energy Research and Development Authority, Northeast Utilities Service Company, Ontario Hydro, Southern California Edison Company, The Standard Oil Company, and University of Rochester. Such support does not imply endorsement of the content by any of the above parties.

REFERENCES

1. "Short-Wavelength, Single-Shell, Direct-Drive Pellet Designs," LLE Review (this issue).
2. S. Skupsky and K. Lee, *J. Appl. Phys.* **54**, 3662 (1983); LLE Review **19**, 120 (1984).
3. M. C. Richardson, T. R. Boehly, B. A. Brinker, T. C. Bristow, R. S. Craxton, J. A. Delettrez, G. Enright, A. Entenberg, W. Friedman, L. M. Goldman, J. Hoose, R. J. Hutchison, L. Iwan, S. Kacenjar, K. Lee, S. A. Letzring, L. D. Lund, R. S. Marjoribanks, R. L. McCrory, J. M. Miller, J. Rizzo, W. D. Seka, S. Skupsky, J. M. Soures, C. P. Verdon, D. M. Villeneuve, E. A. Williams, and B. Yaakobi, in *Laser Interaction and Related Plasma Phenomena*, edited by H. Hora and G. K. Miley (Plenum, New York, 1984), Vol. 6, p. 903; M. C. Richardson *et al.*, in *Plasma Physics and Controlled Nuclear Fusion Research 1982* (IAEA, Vienna, 1983), p. 477; LLE Review **10**, 11 (1982).
4. LLE Review **20**, 150 (1984).
5. LLE Review **17**, 7 (1984).
6. R. P. Bossert, S. D. Jacobs, and L. D. Lund, in NBS Special Publication 669: *Proceedings of the 14th Annual Symposium on Optical Materials for High Power Lasers: 1982*, edited by A. Guenther, H. Bennett, B. Newman, and D. Milam (NBS, Colorado, 1984), pp. 118–129.
7. LLE Review **18**, 61 (1984).
8. Y. Kato *et al.*, *Phys. Rev. Lett.* **53**, 1057 (1984).

1.D Synchronization of Two Actively Mode-Locked and Actively Q-Switched Oscillators

For the recently upgraded GDL laser system¹ to be used as a synchronized x-ray backlighting source for laser-fusion experiments on the 24-beam OMEGA system, it has become necessary to modify the present active-passive mode-locked oscillators² into synchronizable, actively mode-locked and Q-switched oscillators (AMQO). The oscillator is based on a Lawrence Livermore National Laboratory (LLNL) design;³ the opto-mechanical elements of this oscillator, however, were completely redesigned to meet the particular needs of LLE.^{4,5} The application of the LLNL approach to synchronization of multiple oscillators was not straightforward, as the GDL and OMEGA oscillators are physically separated by ≈ 75 m. In addition, the original rf electronics proved too sensitive to electromagnetic interference (EMI) to be operated reliably in our laboratory environment. Because of these factors, it became necessary to redesign this part of the oscillator.

In this article we describe the basic principles,⁵ design criteria, and performance characteristics of the new rf electronics for the AMQO. Also discussed are novel diagnostics and synchronization data. The opto-mechanical design is given elsewhere.^{4,5}

AMQO RF Electronics

In the new design all low-level rf analog signal processing was replaced by CMOS integrated circuit technology because of its high noise immunity. Furthermore, advanced Schottky TTL was used where very high speed was required. Careful design, layout, grounding, and shielding practices make this new design very resistant to EMI.

There is one master rf oscillator, which provides the synchronization for all the oscillators and for a number of relevant timing signals. The rf synchronization is designed around a stable quartz crystal oscillator operating at 66 MHz; the repetition rate signal is obtained from amplitude modulation of the rf. Each one of the separate remote rf control and timing units then detects the leading edge of this amplitude modulation. All other timing signals are generated internally in the remote-control unit, using the phase of the 66-MHz rf or the leading edge of the modulated rf.

One of the remote-control units is designated the master unit, to which all others are slaved. This is a result of a peculiarity of the design, since the total delay of the q-switch pulse with respect to the repetition rate pulse is of the order of milliseconds and its adjustability should be of the order of nanoseconds. (This nanosecond precision proved difficult and a resolution of $\pm 1 \mu\text{s}$ was chosen instead.) However, if each remote unit were to generate its own q-switch pulse, the resulting optical pulse trains would also be afflicted by a microsecond jitter, making oscillator synchronization impossible. Thus, the q-switch pulse generated by the master control unit is routed to the slave units, triggering the q-switch pulses in those units with less than 50-ps jitter. The jitter between the actual optical pulses (from different

oscillators) in the AMQO pulse train primarily depends on the short-term (ms) phase stability of the rf to the acousto-optic mode-locker. This short-term frequency stability has been measured to be approximately 10 ppm/ms. In addition, the remote control units contain three independent high-precision delay units—for triggering, for instance, the single-pulse switch-out electronics (Pockels cell drivers) or streak cameras. These delay generators have a least-count resolution of 16 ns and a measured jitter of 30–40 ps between any two delay generators within a control unit as well as between control units.

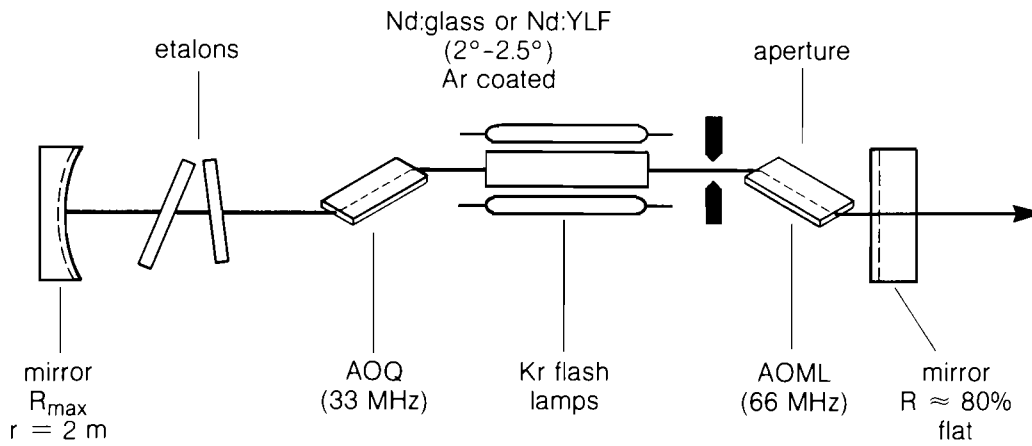
The concept of AMQO's separated physically by long distances and driven by remote rf control units with their proper rf amplifiers requires extraordinary amplitude and phase stability of the rf link between master rf oscillator and control units. To achieve a 30-ps optical pulse jitter between two different AMQO's, we require a phase stability of 1 mrad and an amplitude stability of 0.1%. Given the long distances and the adverse environment with several °C temperature fluctuations, such stability can only be achieved through the use of very high quality cable⁶ with phase stability of 2 to 3 ppm/°C instead of the 200 to 300 ppm/°C for usual coax cable. (The latter would lead to 90 ps/°C optical pulse jitter.) This special cable also has very low loss characteristics (1.2 db/100 ft at 66 MHz), thus satisfying both phase and amplitude stability requirements for the transmission of the rf signal to the remote-control units.

Another major change was made in the design of the flash-lamp driver power supply. This power supply furnishes starting pulse, simmer and boost simmer current pulses, as well as the main lamp discharge pulse. The original design was limited to a peak current of 40 A and required water cooling of more than 40 high-power transistors. This power supply was redesigned using new convection-cooled power transistor modules instead of the water-cooled transistor bank. This also allowed delivery of up to 60-A peak discharge current in a flat-top pulse. The overall reliability of the system was also significantly increased by these design changes.

AMQO Performance

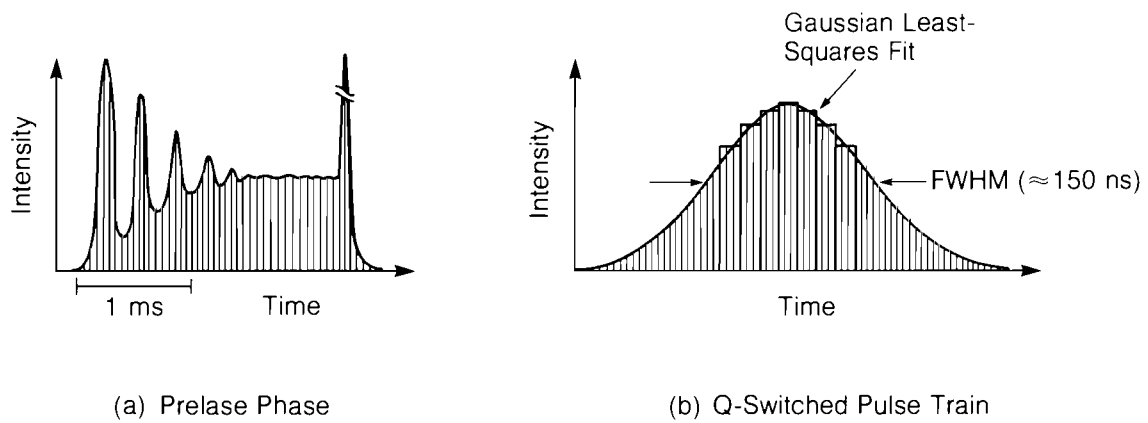
In order to better understand the data below, a brief description of the AMQO is necessary. Figure 23.5 shows the mechanical layout of the oscillator, whose overall length is ≈ 1.2 m. The laser host is Nd:phosphate glass (KIGRE Q-100, 4-mm diam \times 100-mm length). The acousto-optic modulators are fabricated in-house⁴ and operate at 66 MHz (mode-locker, AQML) and 33 MHz (q-switch, AOQ). A typical pulse train, including pre-lasing, is shown in Fig. 23.6. Due to the relatively low gain and slope efficiency of the glass laser host as compared to Nd:YLF or Nd:YAG, the output energy of the oscillator is limited to 40 – 70 μ J per single pulse. However, the output beam has a high-quality intensity distribution (see beam-intensity contour plot in Fig. 23.7) and contrast⁷ ($\geq 10^5$).

The repetition rate for these oscillators is limited to 0.5 Hz due to the poor thermal conductivity of the glass laser host. (In fact, for OMEGA and GDL, the oscillators are expected to be operating at 0.1 Hz.)



E3672

Fig. 23.5
Schematic layout of the major optical components of the AMQO. (AOML: acousto-optic mode-locker; AOQ: acousto-optic q-switch).



E3689

Fig. 23.6
Typical pulse train obtained with an AMQO. (a) The prelude phase, with its characteristic relaxation oscillations. (b) The q-switched pulse train along with the computer characterization.

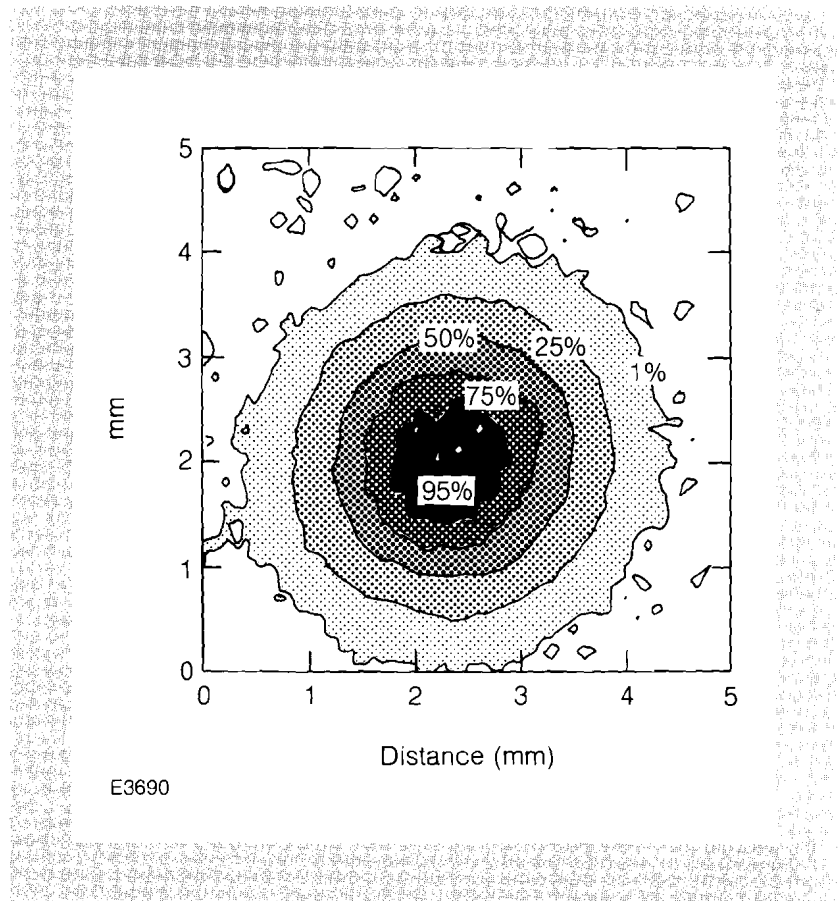
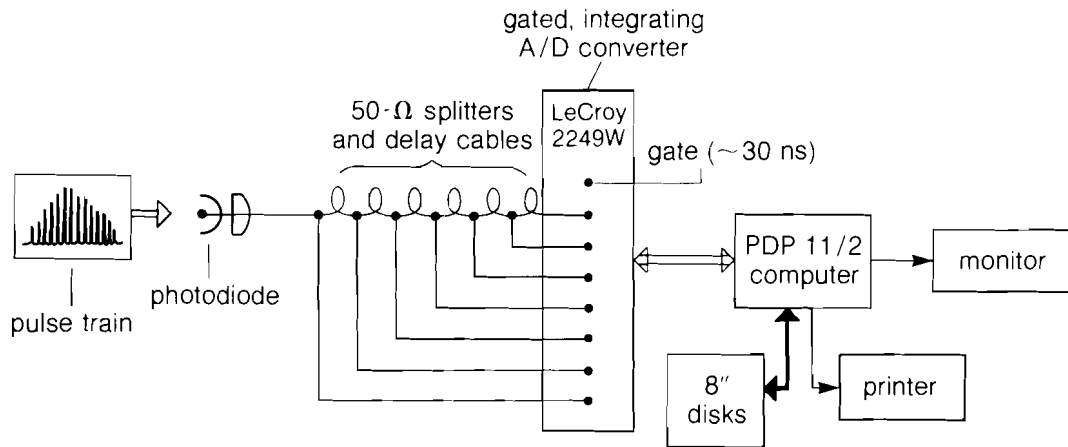


Fig. 23.7
Intensity contour plot of the AMQO output beam with glass laser host. We note the highly symmetric profile, which has been shown to be Gaussian over more than two decades using a diode array.

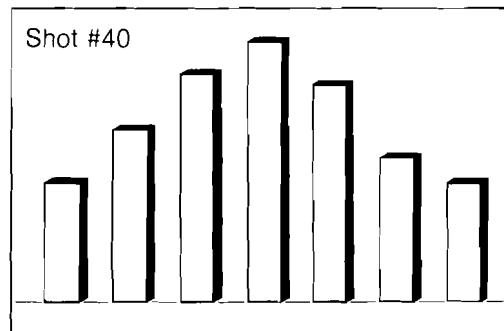
To facilitate AMQO performance evaluation we have developed a novel diagnostic method using a photodiode and a multichannel-gated integrated A/D converter (LeCroy model 2249W), which is coupled to a PDP11/2 computer. The block diagram for this setup is shown in Fig. 23.8. A small part of the oscillator output is incident on a fast photodiode (HP4202, $t_r \approx 1$ ns); it is split seven ways, with cable delays set up between the 50- Ω splitters in such a way that a "coarse" image of the pulse train can be reconstructed by the computer from the gated A/D signals (Fig. 23.9). Each pulse train is analyzed by fitting a Gaussian envelope using a least-squares fitting routine, which yields a measure of the pulse energy at the peak of the train, the FWHM of the train, and the position of the peak of the train. After averaging, the standard deviation of the peak position yields the jitter of the pulse train envelope with respect to the q-switch initiation signal. This diagnostic has proven operationally very useful since it rapidly signals any malfunctioning of the oscillator.

Typical fluctuations of the peak and the FWHM of the pulse train envelope range between 1% and 3% while the jitter of the pulse train maximum is 15 - 20 ns for a FWHM of 350 ns. We note that the length of the pulse train depends on such parameters as the pump power, the q-switch level, and the laser host; it is therefore very different for different laser materials such as glass, YLF, or YAG.



E3673

Fig. 23.8
Block diagram for computerized pulse train monitor. The pulse train seen by the diode is split, delayed, and integrated by a LeCroy-2249W-gated, integrating analog-to-digital converter.



| | last shot | average | std. deviation |
|---------------|-------------|-------------|----------------|
| Single pulse | 50 μ J | 45 μ J | 1% |
| Train energy | 750 μ J | 728 μ J | 1% |
| FWHM | 358 ns | 348 ns | 5% |
| Max. position | 400 ns | 415 ns | 5 ns |

E3674

Fig. 23.9
Typical display obtained with computerized pulse train monitor. The standard deviation of the position of the pulse train maximum is also the jitter of the pulse train envelope. The statistics shown here are for typical performance of well aligned AMQO. The averages and standard deviation are obtained over 50 successive shots.

AMQO Synchronization

Synchronizing two separate AMQO's requires not only rf synchronization (pulse-to-pulse synchronization) but also pulse train envelope synchronization, to at least 10% of the FWHM of the pulse train. The pulse train monitor described above permits verification and quantitative measurement of the envelope synchronization. For the pulse-to-pulse synchronization we used a streak camera in a novel configuration.

The OMEGA and GDL oscillators typically operate in very different pulse-length regimes (OMEGA: $t_p \approx 1$ ns; GDL: $t_p \approx 0.1$ ns) for experimental reasons related to laser fusion and x-ray backlighting. This allows an experimental setup and pulse display on a picosecond streak camera as shown in Fig. 23.10, where A and B are the first and second pulses of the pulse train generated by the 95% etalon (pulse stacker) in the diagnostic beam from the short-pulse oscillator.

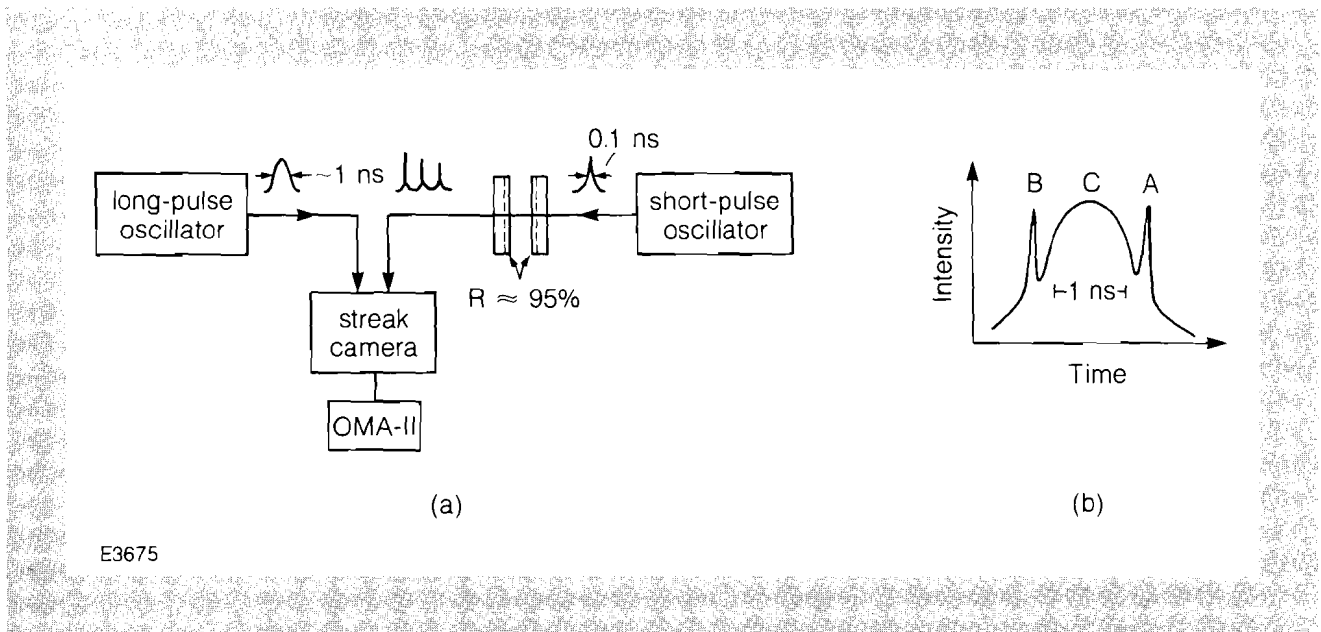


Fig. 23.10

(a) Schematic diagram for streak camera setup for jitter measurements from two oscillators with vastly different pulse durations. The OMA-II is a commercial, optical multichannel analyzer (EG&G-PAR).
 (b) Schematic display of Gaussian pulses for optimum jitter measurements. The short pulses are positioned close to the half-intensity points of the long pulse.

The pulses also provide autocalibration of the time axis of the streak record. The pulse from the long-pulse oscillator (C) is timed to fall in between A and B. The synchronization jitter between the two laser pulses can then be obtained from the position of the three pulses on successive shots. Alternatively, measuring the ratio of the peaks A and B also allows determination of the synchronization jitter since the placement of A and B at about the half-intensity points of C renders this ratio very sensitive to the jitter, as seen in Fig. 23.11. An analysis of a representative series of shots, using the two methods just described, yielded a pulse-to-pulse jitter for the long-pulse and short-pulse oscillators of approximately 22 and 29 ps.

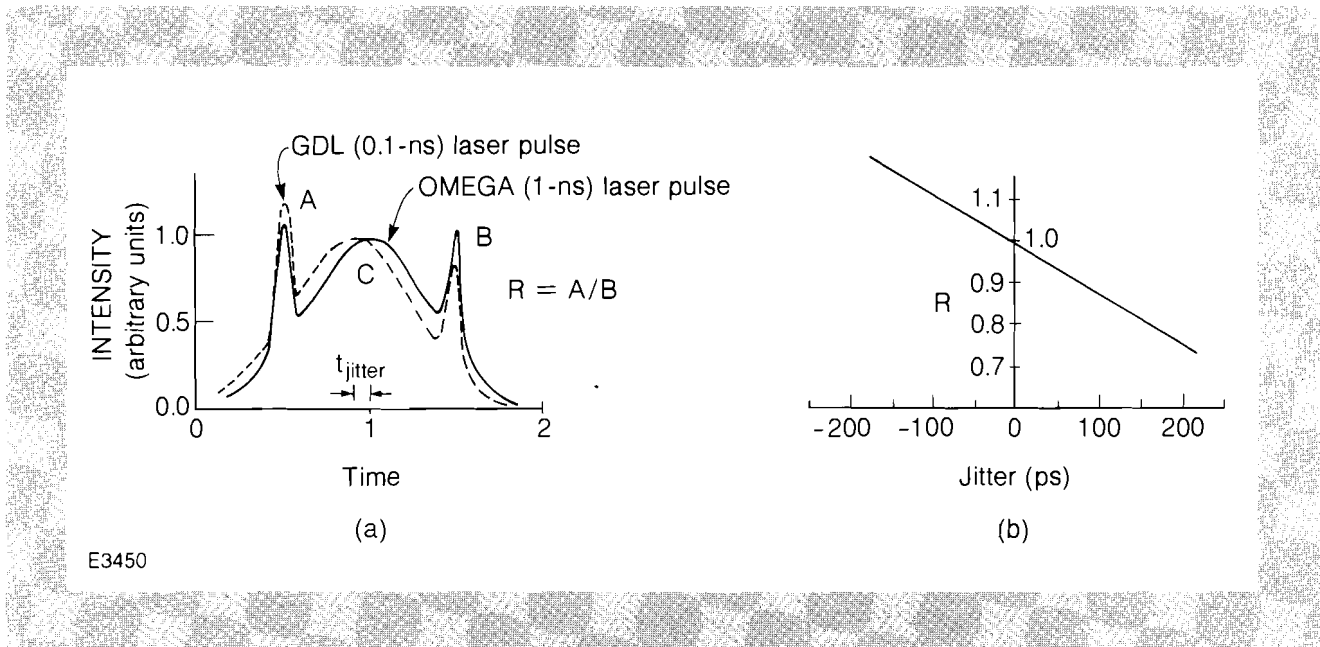


Fig. 23.11

(a) Display of actual streak record corresponding to the setup shown in Fig. 23.10. (b) Dependence of the ratio $R = A/B$, where A and B are the peak intensities of the two short pulses in (a). The straight line in (b) varies only slightly in slope for varying relative intensities between the short and long pulse or their half-widths.

The 20- to 30-ps jitter data between the two AMQO pulses are sufficient for synchronized OMEGA/GDL experiments. So far, we have not determined the source of this jitter or its ultimate limit. However, the present values appear to be close to the instrumental limit for measuring the relative timing of two pulses of vastly different pulse durations. On the other hand, mechanical vibrations of some AOML components at or below the kHz regime at amplitudes around $0.5 \mu\text{m}$ could also account for the 20- to 30-ps jitter. Our present experimental setup is not optimal in this regard and could conceivably contribute significantly to the present jitter measurements.

ACKNOWLEDGMENT

This work was supported by the U.S. Department of Energy Office of Inertial Fusion under agreement number DE-FC08-85DP40200 and by the Laser Fusion Feasibility Project at the Laboratory for Laser Energetics, which has the following sponsors: Empire State Electric Energy Research Corporation, General Electric Company, New York State Energy Research and Development Authority, Northeast Utilities Service Company, Ontario Hydro, Southern California Edison Company, The Standard Oil Company, and University of Rochester. Such support does not imply endorsement of the content by any of the above parties.

REFERENCES

1. LLE Review **21**, 1 (1984).
2. W. Seka and J. Bunkenburg, *J. Appl. Phys.* **49**, 2277 (1978).
3. D. J. Kuizenga, *IEEE J. Quantum Electron.* **17**, 1694 (1981).
4. G. F. Albrecht, L. Lund, and D. Smith, *Appl. Opt.* **22**, 1276 (1983).
5. G. F. Albrecht, M. Grueneisen, and D. Smith, accepted for publication in *IEEE J. Quantum Electron.* (1985).
6. Andrew 35422-9 phase stabilized air dielectric HELIX cable.
7. G. F. Albrecht, *Opt. Commun.* **41**, 287 (1982).